Asymmetric Unsteady Flow in Forward-Facing Cavities

Lars E. Ericsson*
Lockheed Missiles & Space Company, Inc., Sunnyvale, Calif.

An analysis has been performed of the flow oscillation observed in the "empty" nozzles of the space shuttle solid rocket motors (SRM's) after they have been jettisoned at burnout. The unsteady flow phenomenon is similar in many respects to the flow oscillations observed on bodies with flow separation spikes. Hence, a previously developed analytic method for prediction of the spiked-body oscillation frequency has been extended to apply to forward-facing cavities. The predicted frequencies are in good agreement with experimental results. Furthermore, a simple time history analysis produces time-average loads on the forward-facing SRM nozzles that agree well with the observed discontinuous load changes caused by the flow oscillation. The analytic methods have direct or indirect application to analysis of inlet dynamics, supersonic control buzz, and nosetip aerodynamics of ablating re-entry vehicles.

Nomenclature

A = axial force: coefficient $C_A = A/(\rho_\infty U_\infty^2/2)S$
a = speed of sound
c = reference length (SRM diameter)
D = volumetric mean nozzle diameter (Fig. 9)
d_i, D_I = internal nozzle diameters (Fig. 10)
f = oscillation frequency
h_C = cavity depth (Fig. 9)
L_S = spike length for flat-faced bodies
M = Mach number, $M = U/a$
M_p = pitching moment: coefficient $C_m = M_p/(\rho_\infty U_\infty^2/2)Sc$
N = normal force: coefficient $C_N = N/(\rho_\infty U_\infty^2/2)S$
p = static pressure: coefficient $C_p = (p-p_\infty)/(\rho_\infty U_\infty^2/2)$
p_0 = blast wave pressure: coefficient $C_{p0} = (p_0-p_\infty)(\rho_\infty U_\infty^2/2)$
$S_D, S_{LS}, \bar{S}_{LS}$ = Strouhal numbers: $S_D = fD/U_\infty$, $S_{LS} = fL_S/U_\infty$, $\bar{S}_{LS} = f(L_S+h_C)/U_\infty$
T = oscillation period
t = time
Δt = time lag
U = axial velocity
$V_\perp$ = velocity component normal to surface element
X_l = parameter defined in Eq. (1)
x = axial body-fixed coordinate (Fig. 10)
α = angle of attack
α' = α-complement = $\pi - \alpha$
γ = ratio of specific heats = 1.4 in air
Δ = increment
Δ_{sh} = shock standoff distance
θ_R = slope of nozzle wall (Fig. 10)
ρ = air density
φ = azimuth (Fig. 10)
φ' = φ value for Newtonian shadow, Eq. (5)

Subscripts

crit = critical
d = downstream
E = external
I,i = internal
l = linear, tangential extension
max. = maximum
S = spike
SRM = solid rocket motor
u = upstream
∞ = freestream condition

Superscripts

$(\bar{\ })$ = barred quantities denote integrated mean or time-average values
$(\hat{\ })$ = caret indicates value behind a normal shock
$(\check{\ })$ = inverted caret indicates embedded Newtonian value

Presented as Paper 78-54 at the AIAA 16th Aerospace Sciences Meeting, Huntsville, Ala., Jan. 16-18, 1978; submitted March 9, 1978; revision received Aug. 1, 1978.

Index categories: Nonsteady Aerodyanmics; Supersonic and Hypersonic Flow; Jets, Wakes, and Viscid-Inviscid Flow Interactions.

*Consulting Engineer. Associate Fellow AIAA.

Introduction

ACCORDING to present plans, the solid rocket motors (SRM's) of the space shuttle launch vehicle are to be jettisoned after burnout and recovered for renewed usage.[1] Consequently, wind-tunnel tests have been made of the SRM's in the complete angle-of-attack range $0 \le \alpha \le 180$ deg.[2] Recent tests[3] showed that discontinuous changes of the aerodynamic characteristics occur in the α range $140 < \alpha < 180$ deg (Fig. 1). The discontinuous flow change is associated with α-hysteresis (Fig. 1) and pulsating unsteady flow (Fig. 2), all characteristics that have been observed on spiked bodies. Consequently, earlier performed spiked-body analyses[4-8] were extended to include methods for prediction of the unsteady aerodynamics of the pulsating flow phenomenon.

Flow Description

The flow pictures in Fig. 2 and those of a Polaris re-entry body with hollow skirt[9] (Fig. 3) describe the unsteady flow configuration sketched in Fig. 4. When the flow inclination is below a critical value, $\alpha' < \alpha'_{crit}$, stable flow exists. The sketch leaves out any of the recirculatory details in the cavity, which in this case effectively works as a dead air region. When the critical flow inclination is exceeded, $\alpha' > \alpha'_{crit}$, the bowshock "pops" into the cavity and the sketched flow geometry is generated momentarily. This flow geometry is unstable, as the flow turned down from the stagnation region has no way to escape without pushing the deformed bowshock forward until it finally reaches the stable flow location. Then the recirculated mass flow is spilled over the top edge of the nozzle so that the bowshock can pop into the cavity again and the cycle is repeated. Figure 5 shows the flow geometry existing for a spiked cavity at zero angle of attack. Again, the recirculated flow cannot be spilled until the "swallowed" shock system has been pushed forward. In this case the forward movement does not stop until the end of the spike is

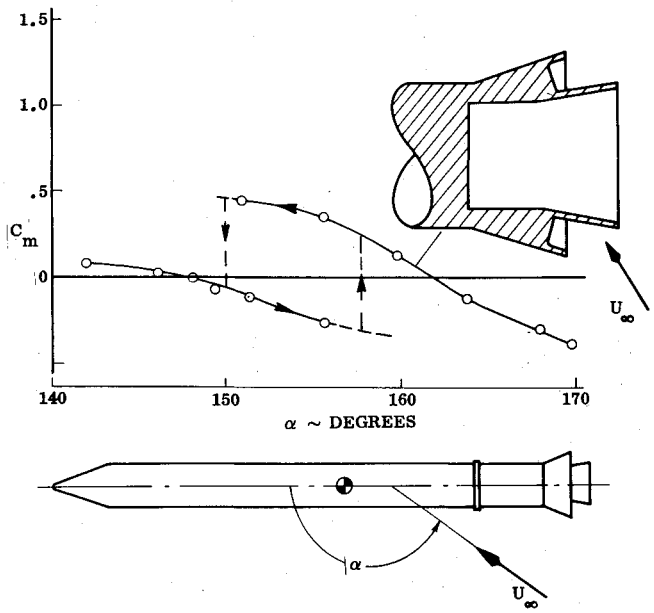

Fig. 1 Pitching moment of SRM at $M_\infty = 3.48$.

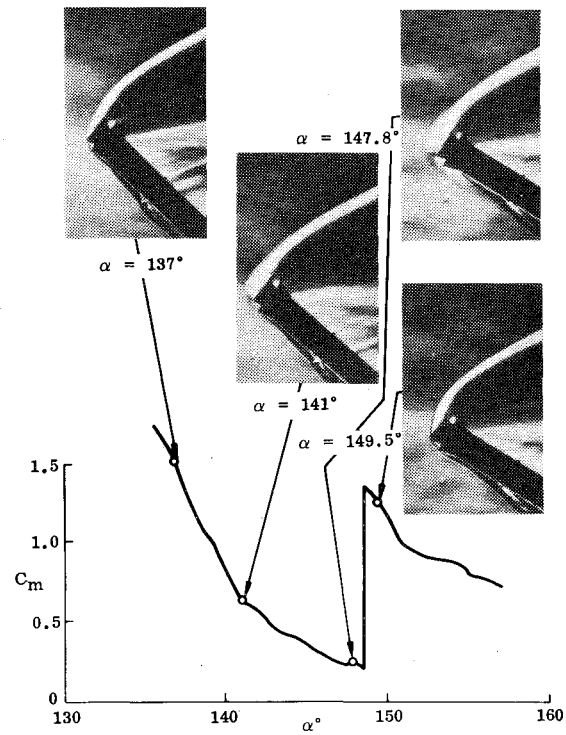

Fig. 2 Shadowgraphs of unsteady flow at $M_\infty = 3.48$ on SRM with nozzle E_{1A}.

reached; then the recirculatory flow is spilled, the shock is swallowed and the cycle starts all over again.

For a spiked body without a cavity, the flow situation is the one sketched in Fig. 6. When the face shoulder is steep, as for the case sketched, no stable flow exists. The secondary shock is a strong detached shock which causes the same unstable recirculatory flow situation discussed earlier. This unsteady spiked-body flow is analyzed in Ref. 8 where analytical means are developed by which the frequency of the flow pulsations can be predicted. The purpose of the present paper is to describe how the analytic methods of Ref. 8 can be modified to apply to the unsteady flow situation sketched in Figs. 4b and 5.

Analytic Approach

The Strouhal number predicted by the analytic method of Ref. 8 for the flow pulsations occurring on a flat-faced spiked body (Fig. 6) is shown in Fig. 7. The dash-dot line in Fig. 7 denotes the limit for the similar flow profile assumption used in Ref. 8. For longer spikes the flow impingement geometry starts to change (see Ref. 8), causing first a change in the type of flow unsteadiness and finally resulting in a stable, retarded spike-induced separation of turbulent flow (Fig. 8). The maximum spike length that will retain laminar flow separation starting at the spike tip (Fig. 6) gives the maximum Strouhal number (shown in Fig. 9 of Ref. 8). This Strouhal number is the asymptotic limit for the predictions in Fig. 7 for spikes longer than $L_S = \Delta_{sh} + 0.45\, L_{S\,\max.}$. However, when the spiked body has a forward-facing, sharp-lipped cavity, as sketched in Fig. 5, the maximum normal-shock-recovered stagnation conditions in the recirculatory flow region are maintained. Thus, the predictions for the Strouhal number of oscillations in spiked cavities are obtained by a tangential extension from the dash-dot line in Fig. 7. Modifying Eq. (19) of Ref. 8 in this manner gives

$$\bar{S}_{LS} = \frac{0.32}{(L_S/D)^{1/2}_{\max.}} \times \begin{cases} 0.26\left[1+3.46\left(\frac{L_S}{D}+\frac{h_C}{D}-\frac{\Delta_{sh}}{D}\right)\right] & \left(\frac{L_S}{D}+\frac{h_C}{D}-\frac{\Delta_{sh}}{D} \le \frac{1}{4}\right) \\ \left(\frac{L_S}{D}+\frac{h_C}{D}-\frac{\Delta_{sh}}{D}\right)^{1/2}\left[1-0.14\left(\frac{L_S}{D}+\frac{h_C}{D}-\frac{\Delta_{sh}}{D}\right)\right] & \left(\frac{1}{4} < \frac{L_S}{D}+\frac{h_C}{D}-\frac{\Delta_{sh}}{D} < X_l\right) \\ \frac{1}{2}\left[X_l^{1/2}(1+0.14X_l)+\frac{1-0.42X_l}{X_l^{1/2}}\left(\frac{L_S}{D}+\frac{h_C}{D}-\frac{\Delta_{sh}}{D}\right)\right] & \left(\frac{L_S}{D}+\frac{h_C}{D}-\frac{\Delta_{sh}}{D} \ge X_l\right) \end{cases} \quad (1)$$

where $X_l = 0.45\,(L_S/D)_{\max.}$

From Ref. 8 one also knows that

$$\left(\frac{L_S}{D}\right)_{\max.} = \begin{cases} 1.6(1+0.1M_\infty) & (M_\infty \le 11.3) \\ 3.4 & (M_\infty > 11.3) \end{cases} \quad (2)$$

and that Δ_{sh}/D, according to Ref. 10, can be approximated as

$$\frac{\Delta_{sh}}{D} = \frac{0.515}{[(\hat{\rho}/\rho_\infty)-1]^{1/2}} \quad (3)$$

where $\hat{\rho}/\rho_\infty$ is the density ratio through a normal shock.

Figure 9 shows that the predictions through Eqs. (1-3) are in good agreement with the experimental results obtained by Hermach et.al.[11] Also shown in Fig. 9 is one data point for the empty SRM shell "flying backwards." In what follows it will be explained how this data point was introduced into the graph of Fig. 9.

In case of the spiked cavity, the most forward extent of the pulsating flow is determined by the spike tip. For the forward-facing pure cavity (Fig. 4), a first approximation for this forward movement is the bowshock location for the steady flow. This also appears to be in good agreement with the flow pictures in Fig. 2. Thus, the SRM nozzle data point in Fig. 9 was obtained from the measured Strouhal number, $(S_D)_{\mathrm{SRM}} = 0.18$, based on the SRM diameter,[3] by converting it to an effective Strouhal number S_{LS} through the following relationship:

$$\bar{S}_{LS} = (S_D)_{\mathrm{SRM}} \frac{D_I}{D_{\mathrm{SRM}}}\left(\frac{h_C}{D_I}+\frac{\Delta_{sh}}{D}\frac{D_E}{D_I}\right) \quad (4)$$

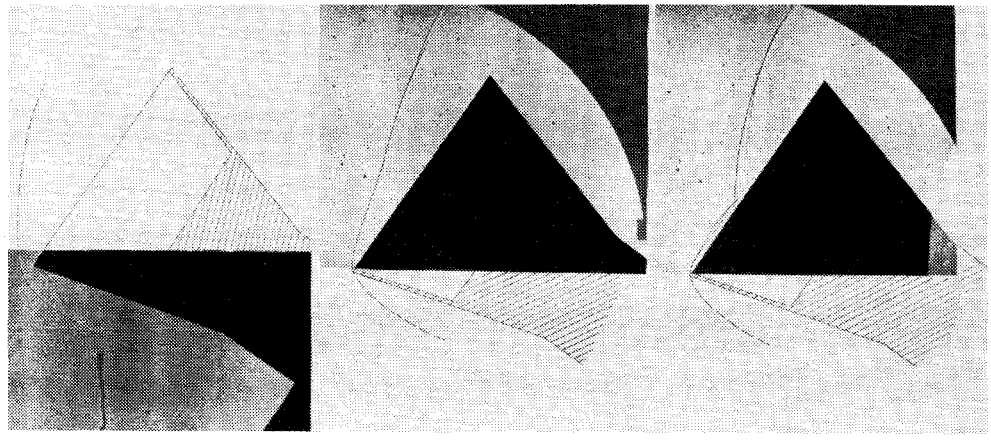

Fig. 3 Shadowgraphs of unsteady flow over forward-facing cavity at 35 deg flow inclination.

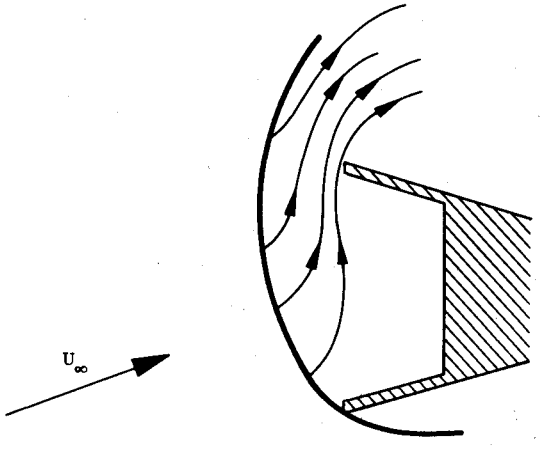

a) $\alpha' < \alpha'_{crit}$. STEADY FLOW

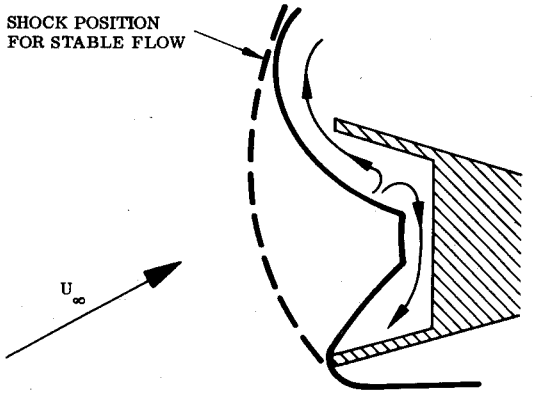

b) $\alpha' > \alpha'_{crit}$. UNSTEADY FLOW

Fig. 4 Steady and unsteady cavity flows.

where Δ_{sh}/D is given by Eq. (3). D_I is the mean† internal nozzle diameter and D_E is the maximum external body diameter in the exit plane (i.e., including skirt). Figure 9 shows that Eqs. (3) and (4) provide good prediction of the measured frequency of the flow pulsations in the rocket nozzle.[3]

Unsteady Aerodynamics

In order to get a first approximation of the loads induced on the SRM's by the pulsations, the flow is idealized as follows. It is assumed that the internal nozzle loads upstream of the swallowed bowshock can be determined with

†Volumewise, that is. It is the diameter marked D in Fig. 9.

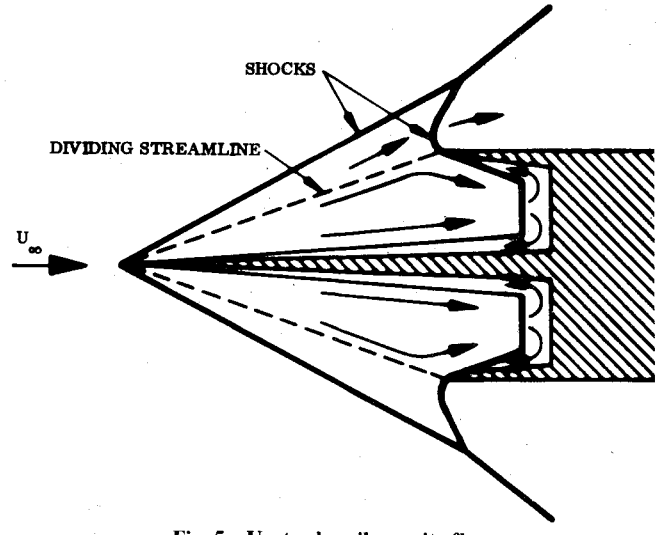

Fig. 5 Unsteady spike-cavity flow.

satisfactory accuracy by embedded Newtonian theory,[12,13] and that the pressure behind the swallowed shock (during the upstroke phase) is given by normal shock relations. Assuming a two-dimensional type behavior for the internal flow, one can, according to Ref. 14, set $\rho U^2 = \rho_\infty U_\infty^2$. C_{p0} is a function of x only, and with $V_\perp / U$ defined as in Ref. 13 with $\theta_F = \theta_R$, one obtains for the nozzle geometry in Fig. 10 the following result:

$$C_{\bar{p}} = \begin{cases} C_{p0} + C_{p_{\max.}} \left(\dfrac{V_\perp}{U_\infty} \right)^2 & (\phi < \Phi') \\ C_{p0} & (\phi' \leq \Phi) \end{cases}$$

$$\frac{V_\perp}{U} = \sin\alpha' \cos\theta_R \sin\phi - \cos\alpha' \sin\theta_R$$

$$\phi' = \sin^{-1} \left(\frac{\tan\theta_R}{\tan\alpha'} \right)$$

$$\alpha' = \pi - \alpha$$

$$C_{p\max.} \approx 1.8 \qquad (5)$$

When the strong shock has passed upstream over the area element, the pressure is given by normal shock relations.[15] In the case of steady hypersonic flow, the shock strength is

$$C_{\bar{p}0} = \frac{4}{\gamma+1} \left(1 - \frac{1}{M_\infty^2} \right) \approx \frac{4}{\gamma+1} \qquad (6)$$

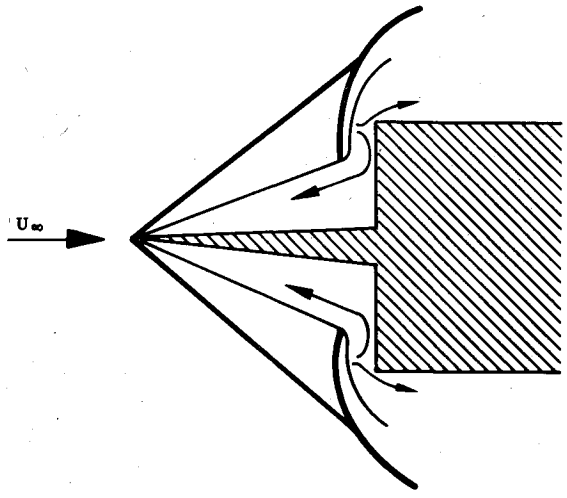

Fig. 6 Unsteady spiked-body flow.

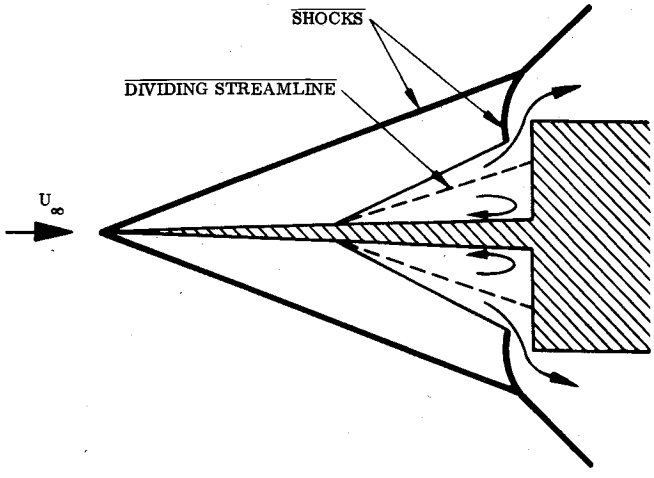

Fig. 8 Retarded spike-induced flow separation.

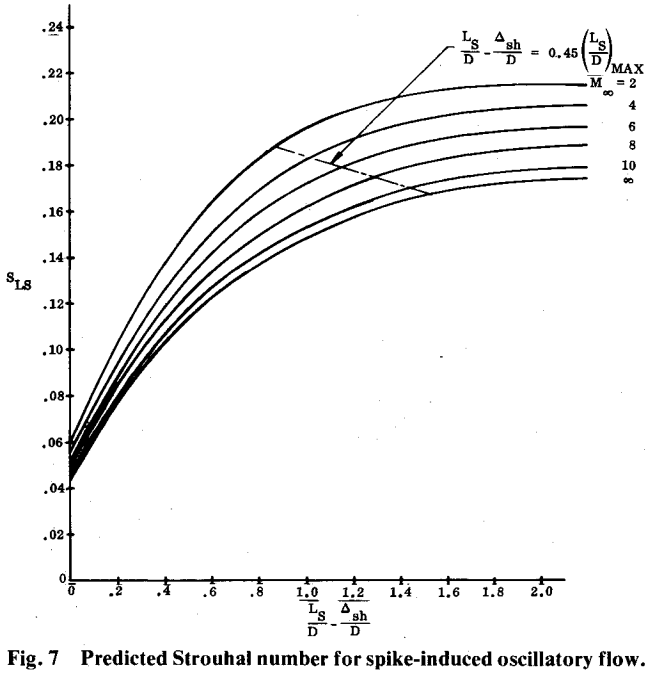

Fig. 7 Predicted Strouhal number for spike-induced oscillatory flow.

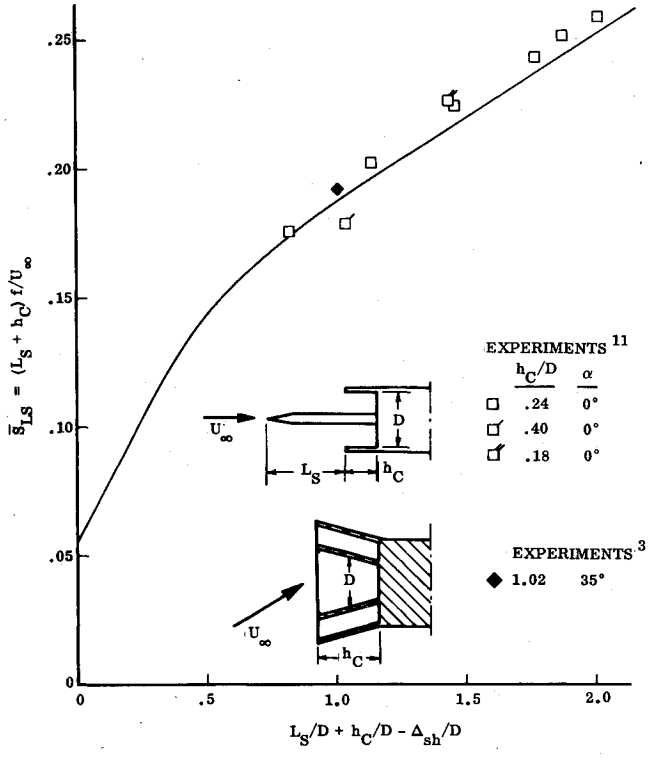

Fig. 9 Predicted and measured frequency of pulsating flow in forward-facing cavities at $M_\infty = 3.5$.

In the nonsteady case the shock strength can be written

$$C_{\hat{p}_{NS}} \approx \frac{4}{\gamma+1}\left(1+\frac{\Delta M_{NS}}{M_\infty}\right)^2 \tag{7}$$

where $\Delta M_{NS} > 0$ for the pumping phase when the shock moves upstream and $\Delta M_{NS} < 0$ for the expansion phase when the shock moves downstream. Thus, the pressure on the internal nozzle wall will vary with time, as is illustrated in Fig. 11. In the steady case, the pressure is $C_{\hat{p}0}$ throughout the nozzle, where $C_{\hat{p}0} < C_{\hat{p}u}$. The pressure change in the unsteady case from the steady-state level is $\Delta C_p = C_p - C_{\hat{p}0}$, where C_p is given by either Eq. (5) or (7). For deeper cavities, the results obtained by Vrebavolich[16] indicate the following values of $C_{\hat{p}u}$ and $C_{\hat{p}d}$:

$$0 < C_{\hat{p}d} < 0.2C_{\hat{p}0}$$

$$C_{\hat{p}u} > C_{\hat{p}0} \tag{8}$$

The strip loading is (see Fig. 10)

$$\frac{d\Delta C_A}{dr} = -\frac{2r}{S} \times \begin{cases} \int_{-\pi/2}^{\pi/2} (C_{\hat{p}u} - C_{\hat{p}0})\, d\phi & (t_0 \le t < t_1) \\ \int_{-\pi/2}^{\pi/2} (C_{\hat{p}d} - C_{\hat{p}0})\, d\phi & (t_1 + \Delta T < t < t_2) \\ \int_{-\pi/2}^{\pi/2} (C_{\hat{p}} - C_{\hat{p}0})\, d\phi & (t_2 \le t \le t_3) \end{cases} \tag{9}$$

$$\frac{d\Delta C_N}{dx} = -\frac{2r}{S} \times \begin{cases} \int_{-\pi/2}^{\pi/2} (C_{\hat{p}u} - C_{\hat{p}0}) \sin\phi\, d\phi & (t_0 \le t < t_1) \\ \int_{-\pi/2}^{\pi/2} (C_{\hat{p}d} - C_{\hat{p}0}) \sin\phi\, d\phi & (t_1 + \Delta T < t < t_2) \\ \int_{-\pi/2}^{\pi/2} (C_{\hat{p}} - C_{\hat{p}0}) \sin\phi\, d\phi & (t_2 \le t \le t_3) \end{cases} \tag{10}$$

Integrating Eqs. (9) and (10) utilizing Eqs. (5-8) gives

$$\frac{d\Delta C_A}{dr} = \frac{2\pi r}{S} \times \begin{cases} C_{\hat{p}0} - C_{\hat{p}u} & (t_0 \le t < t_1) \\ C_{\hat{p}0} - C_{\hat{p}d} & (t_1 + \Delta T < t < t_2) \\ C_{\hat{p}0} - C_{p0} - \dfrac{C_{p\,\max.}}{\pi}\left[\left(\dfrac{\pi}{2} + \phi'\right)\left(\cos^2\alpha' \sin^2\theta_R + \dfrac{1}{2}\sin^2\alpha' \cos^2\theta_R\right) + \dfrac{1}{2}\sin 2\alpha' \sin 2\theta_R \cos\phi'\right] & (t_2 \le t \le t_3) \end{cases} \tag{11}$$

$$\frac{d\Delta C_N}{dx} = \frac{2r}{S} C_{p_{\max.}} \times \begin{cases} 0 & (t_0 \le t < t_1) \\ 0 & (t_1 + \Delta T < t < t_2) \\ \left(\dfrac{\pi}{2} + \phi' - \dfrac{1}{2}\sin 2\phi'\right)\dfrac{1}{4}\sin 2\alpha' \sin 2\theta_R + \cos\phi'\left[\cos^2\alpha' \sin^2\theta_R + \sin^2\alpha' \cos^2\theta_R\left(1 - \dfrac{1}{3}\cos^2\phi'\right)\right] & (t_2 \le t < t_3) \end{cases} \tag{12}$$

From Fig. 11, one can define the time duration during one cycle for the different pressure levels. Assuming that $\Delta T/T$ is negligibly small, one obtains

$$\frac{t_1 - t_0}{T} = \frac{x + \Delta_{sh}}{h_C + \Delta_{sh}}\left(1 + \frac{\bar{U}_u}{\bar{U}_d}\right) \qquad \frac{t_2 - t_1}{T} = \frac{x + \Delta_{sh}}{h_C + \Delta_{sh}}\left(1 + \frac{\bar{U}_d}{\bar{U}_u}\right) \qquad \frac{t_3 - t_2}{T} = \frac{h_C - x}{h_C + \Delta_{sh}} \tag{13}$$

If the nozzle walls are thin or the nozzle lips are relatively sharp, one can neglect C_{p0} (Refs. 13 and 14). Another simplification is obtained by assuming that $\bar{U}_d = U_\infty$. Equations (11-13) then give the following integrated result:

$$\overline{\Delta C_A} = \frac{\pi D_I^2}{12S}\frac{h_C}{(h_C + \Delta_{sh})}\left\{\left\{\left[2 - \frac{d_i}{D_I} - \left(\frac{d_i}{D_I}\right)^2\right]\left\{C_{\hat{p}0} - \frac{C_{p\,\max.}}{\pi}\left[\left(\frac{\pi}{2} + \phi'\right)\left(\cos^2\alpha' \sin^2\theta_R + \tfrac{1}{2}\sin^2\alpha' \cos^2\theta_R\right)\right.\right.\right.$$
$$\left.\left.\left. + \tfrac{1}{2}\sin 2\alpha' \sin 2\theta_R \cos\phi'\right]\right\} + \left[1 + \frac{d_i}{D_I} + \left(\frac{d_i}{D_I}\right)^2 + 3\frac{\Delta_{sh}}{h_C}\right]\left[(C_{\hat{p}0} - C_{\hat{p}u}) + \frac{\bar{U}_u}{\bar{U}_d}(C_{\hat{p}0} - C_{\hat{p}d})\right]\Big/\left(1 + \frac{\bar{U}_u}{\bar{U}_d}\right)\right\}\right\} \tag{14}$$

$$\overline{\Delta C_N} = \frac{h_C D_I}{6S}\frac{h_C}{(h_C + \Delta_{sh})}\left(2 + \frac{d_i}{D_I}\right)C_{p\,\max.}\left\{\left(\frac{\pi}{2} + \phi' - \tfrac{1}{2}\sin 2\phi'\right)\tfrac{1}{4}\sin 2\alpha' \sin 2\theta_R\right.$$
$$\left. + \cos\phi'\left[\cos^2\alpha' \sin^2\theta_R + \sin^2\alpha' \cos^2\theta_R\left(1 - \tfrac{1}{3}\cos^2\phi'\right)\right]\right\} \tag{15}$$

The corresponding change of the pitching moment is

$$\overline{\Delta C_m} = \overline{\Delta C_N}\,(\bar{x} - x_{CG})/c$$
$$\bar{x} = \frac{h_C}{4}\left(1 + \frac{d_i}{D_I}\right)\Big/\left(1 + \frac{1}{2}\frac{d_i}{D_I}\right) \tag{16}$$

The discontinuous changes of the aerodynamic characteristics caused by the flow pulsations are shown in Fig. 12, complementing the C_m results already shown in Fig. 2. The magnitude of the C_N discontinuity is not measurable; however, the C_A and C_m discontinuities are. Figure 13 shows the measured discontinuities for three different nozzle geometries.[2,3] Also shown are the time-average values predicted from the present analysis.‡ The agreement between predicted and measured discontinuities is very satsifactory, and lends credibility to the very simple unsteady flow model suggested for the pulsating flow process. Thus, it should be possible to use the present model in an analysis to determine whether or not the pulsating flow phenomenon will endanger the structural integrity of the rocket nozzle on the jettisoned, empty SRM shells. The time-average effects are also important in their own right as the associated discontinuous effects on the static or low-frequency characteristics have a decisive impact not only on rigid-body static stability and control but also on the dynamic response of rigid-body and

‡The values used, $C_{\hat{p}d} = 0$ and $C_{\hat{p}u} = C_{\hat{p}0}$, give a high estimate of ΔC_A.

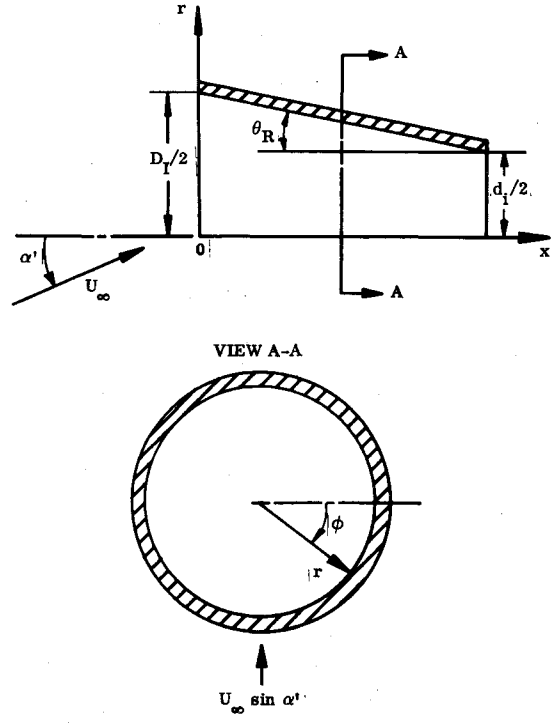

Fig. 10 Definition of nozzle geometry.

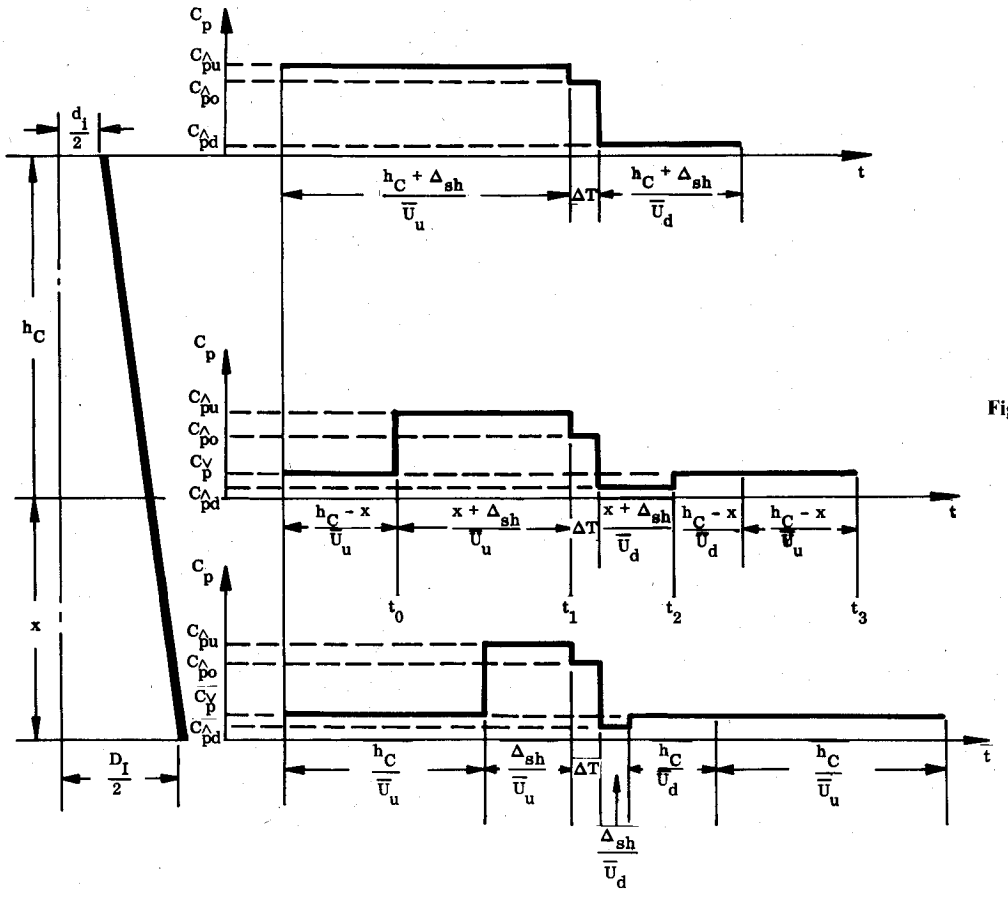

Fig. 11 Idealized pressure time history.

low-frequency elastic modes. The asymmetric oscillatory flow experienced by the forward-facing empty nozzles at high angle of attack[2,3,9] (Figs. 2 and 3) has also been observed on a spiked body[17]§ and could conceivably also occur on the "proboscidean" nosetip of a re-entry vehicle,[8,18,19] causing discontinuous time-average effects similar to those shown in Figs. 1, 2, 12, and 13. In some cases the pulsating flow phenomenon with its strong normal shock (Figs. 2 and 3) may not be realized, but rather the flow oscillation involving a weaker conic shock. However, the convective flow processes should still remain the same, as indicated by the experiment performed by Kabelitz.[19,20] Thus, the analytic methods developed in Ref. 8 and extended in the present paper should be applicable also to the flexing conical shock oscillation.

A phenomenon that involves the flexing shock oscillation is hypersonic control buzz. Mair[21] showed that the two-dimensional equivalent to a spiked body, i.e., the forward-facing step, also could experience the pulsating flow phenomenon. In Mair's case the aspect ratio of the flap or forward-facing step was infinite. Even for finite aspect ratio, however, where the separated flow region can be vented by sideways bleed, shock oscillations have been observed. Goldman and Obremsky[22] observed shock oscillations of the flexing type on a delta planform space vehicle. The oscillations existed for a wide range of control deflections and angles of attack. The spectrum of the oscillation pressure in the separated flow region showed a pronounced harmonic spike at a frequency that produces a Strouhal number based on effective 2-D spike length that is of similar magnitude as that for the spike-induced oscillations discussed earlier. Thus, one can feel confident that the presented methodology could be applied also to this control-buzz phenomenon. Of course, the crossflow relief has to be accounted for. However, this could be accomplished using static experimental data in a manner similar to what is done in Ref. 8.

§In this case the oscillation was, however not of harmonic nature.

Large flexing shock oscillations have also been observed[23] when the hypersonic control consists of a lateral jet. The frequency is according to the authors of a magnitude comparable to that for spiked-body oscillations. It will, of course, be somewhat more difficult to extend the present methods to cover this "fluid control buzz" phenomenon, mainly because of the difficulty to obtain the needed "static" experimental data.

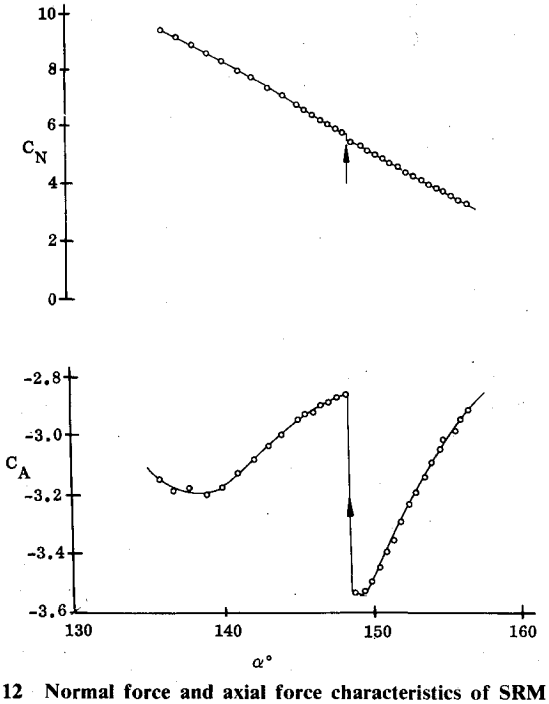

Fig. 12 Normal force and axial force characteristics of SRM with nozzle E_{1A} at $M_\infty = 3.48$.

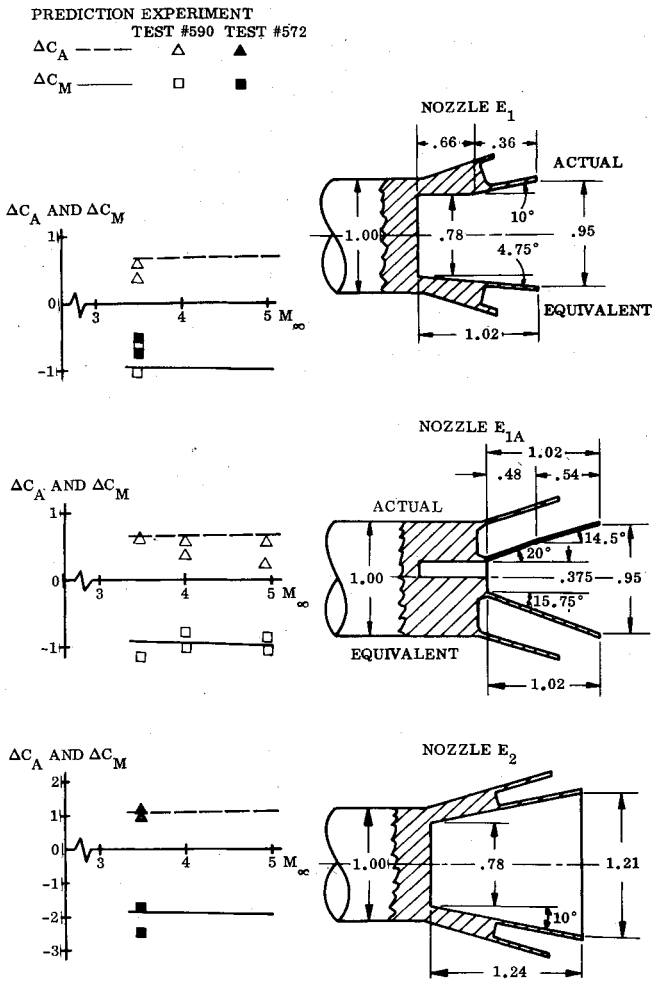

Fig. 13 Comparison between predicted and measured aerodynamic discontinuities for three different SRM nozzles.

Conclusions

The main results of a study of asymmetric unsteady supersonic flow phenomena in forward-facing cavities are as follows:

1) Unsteady flow exists in forward-facing cavities at moderately high flow inclinations (at which the windward branch of the bowshock moves into the cavity). The phenomenon is very similar to that observed at zero flow inclination in cavities with a flow separation spike present.

2) Simple analytic means have been developed by which the experimentally observed oscillation frequency of the pulsating flow can be predicted for forward-facing cavities with and without flow separation spikes.

3) The postulated mathematical model for the pressure time history of the pulsating flow gives time-average results that are in good agreement with the measured discontinuities in the aerodynamic characteristics of the space shuttle SRM's.

It appears that the developed analytic means could with little difficulty be extended to deal with supersonic control buzz and nosetip aerodynamics of ablating re-entry vehicles. It may also be fruitful to take another look at inlet buzz in light of these new results.

References

[1] Fink, D.A.. "Space Shuttle Flight Plan Written," *Aviation Week & Space Technology*, June 3, 1974, pp. 12-15.

[2] Johnson, J.D. and Radford, W.D., "Aerodynamic Characteristics of a 142-Inch Diameter Solid Rocket Booster," NASA CR-128, 774, Aug. 1973.

[3] Clever, W.W., Private communication of unpublished data, NASA Marshall Space Flight Center, Nov. 1975.

[4] Ericsson, L.E. and Reding, J.P., "Analysis of Flow Separtion Effects on the Dynamics of a Large Space Booster," *Journal of Spacecraft and Rockets*, Vol. 2, July-Aug. 1965, pp. 481-590.

[5] Ericsson, L.E. and Reding, J.P., "Dynamics of Separated Flow over Blunt Bodies," Lockheed Missiles & Space Company, Inc., Sunnyvale, Calif., Tech. Summary Rept. 2-80-65-1, Contract NAS 8-5338, Nov. 1962

[6] Ericsson, L.E., "Unsteady Characteristics of a Spiked Bluff Body," Lockheed Missiles & Space Company, Inc., Sunnyvale, Calif., LMSC-804651, Contract NAS 8-5338, July 1964.

[7] Ericsson, L.E., "Steady Loads on Spiked Blunt Bodies of Revolution," Lockheed Missiles & Space Company, Inc., Sunnyvale, Calif., LMSC TM 53-40-121 (LMSC-A312114), Contract NAS 8-5338, Nov. 1962.

[8] Ericsson, L.E., "Flow Pulsations on Concave Conic Forebodies," *Journal of Spacecraft and Rockets*, Vol. 15, July-Aug. 1978, pp. 287-292.

[9] Navone, M.V., "Results of Pressure Tests on Rearward Facing Polaris Reentry Bodies in the AEDC/VKH Tunnel B (R-103)," Lockheed Missiles & Space Company, Sunnyvale, Calif., TM 57-11-67, LMSC/656605, June 1962.

[10] Serbin, H., "Supersonic Flow Around Blunt Bodies," *Journal of Aerospace Sciences*, Vol. 25, Jan. 1958, pp. 58-59.

[11] Hermach, C.A., Kraus, S., and Reller, J.O., Jr., "Reduction in Temperature-Recovery Factor Associated with Pulsating Flows Generated by Spike-Nosed Cylinders at Mach Number of 3.50," NACA RM A56L05, March 1957.

[12] Ericsson, L.E., "Unsteady Embedded Newtonian Flow," *Astronautica Acta*, Vol. 18, Nov. 1973, pp. 309-330.

[13] Ericsson, L.E., "Generalized Unsteady Embedded Newtonian Flow," *Journal of Spacecraft and Rockets*, Vol. 12, Dec. 1975, pp. 718-726.

[14] Ericsson, L.E., Almroth, B.O., Bailie, J.A., Brogan, F.A., and Stanley, G.M., "Hypersonic Aeroelastic Analysis," LMSC Rept. LMSC-D056746, Contract N62269-73C-0713, Sept. 1975.

[15] Ames Research Staff, "Equations, Tables, and Charts for Compressible Flow," NACA Rept 1135, 1953.

[16] Vrebalovich, T., "Resonance Tubes in a Supersonic Flow Field," Jet Propulsion Lab. TR/No. 32-378, July 1962.

[17] Guenther, R.A. and Reding, J.P., "Fluctuating Pressure Environment of a Drag Reduction Spike," AIAA Paper 77-90, Los Angeles, Calif., Jan. 1977.

[18] Chen, K.K., Pallone, A.J., and Thyson, N., "Types of Nosetip Shape Change During Atmospheric Entry," AIAA 7th Fluid and Plasma Dynamics Conference, Palo Alto, Calif., June 1971.

[19] Kabelitz, H-P., "Zur Stabilität geschlossener Grentzschichtablösegebiete an konischen Drehkörpern bei Hyperschallanströmung," DLR FB 71-77, July 1971.

[20] Kabelitz, H-P., "Zur Stabilität geschlossener Grenzschichtablösegebiete bei Über-und Hyperschallanströmung," Vortrags-Nr. 71-065, 4. Jahrestagung der DGLR, Baden-Baden, W. Germany, Oct. 1971.

[21] Mair, W.A., "Experiments on Separation of Boundary Layers on Probes in Front of Blunt-Nosed Bodies in a Supersonic Air Stream," *Philosophical Magazine*, Vol. 43, 1952, pp. 695-716.

[22] Goldman, R.L. and Obremsky, H.J., "Experimental Investigation of Hypersonic Buzz on a Delta Configuration," *AIAA Journal*, Vol. 11, Oct. 1973, pp. 1361-1362; also AIAA Paper 73-157, Jan. 1973.

[23] Rosenbaum, H., Siegelman, D., and Boger, R.C., "Flowfield Interactions Induced by Massive Lateral Injection," *AIAA Journal*, Vol. 13, Nov. 1975, pp. 1441-1447.